Sulfate-controlled Heterogeneous $CaCO_3$ Nucleation and Its Non-linear Interfacial Energy Evolution

Yaguang Zhu,[1] Qingyun Li,[1,*] Doyoon Kim,[1,†] Yujia Min,[1,‡] Byeongdu Lee,[2] and Young-Shin Jun[1,*]

[1]*Department of Energy, Environmental & Chemical Engineering, Washington University in St. Louis, St. Louis, Missouri 63130, United States*

[2]*X-ray Science Division, Argonne National Laboratory, Argonne, Illinois 60439, United States*

E-mail: ysjun@seas.wustl.edu

http://encl.engineering.wustl.edu/

Submitted: May 2021

Revised: June 2021

Environmental Science & Technology

*To Whom Correspondence Should be Addressed

[*]Current address: SLAC National Accelerator Laboratory, Stanford University, CA 94305, USA

[†]Current address: Department of Civil and Environmental Engineering, Massachusetts Institute of Technology, Cambridge, MA 02139, USA

[‡]Current address: Department of Civil Environmental and Geodetic Engineering, The Ohio State University, Columbus, OH 43210, USA

Abstract

Unveiling the effect of an environmental abundant anion "sulfate" on the formation of calcium carbonate ($CaCO_3$) is essential to understand the formation mechanisms of biominerals like corals and brachiopod shells, as well as the scale formation in desalination systems. However, it was experimentally challenging to elucidate the sulfate–$CaCO_3$ interactions at the explicit first step of $CaCO_3$ formation: nucleation. In addition, there is limited quantitative information on the precise control of nucleation kinetics. Here, heterogeneous $CaCO_3$ nucleation is monitored in real time as a function of sulfate concentrations (0–10 mM Na_2SO_4), using synchrotron-based grazing incidence X-ray scattering techniques. The results showed that sulfate can incorporate in the nuclei, resulting in a nearly 90% decrease in the $CaCO_3$ nucleation rate, causing a 120% increase in $CaCO_3$ nucleus size, and inhibiting the vaterite to calcite phase transformation. Moreover, this work quantitatively relates sulfate concentrations to the effective interfacial energies of $CaCO_3$ and finds a non-linear trend, suggesting $CaCO_3$ heterogeneous nucleation is more sensitive at a low sulfate concentration. The study can be readily extended to study other additives and obtain quantitative relationships between additive concentrations and $CaCO_3$ interfacial energies, a key step towards achieving natural and engineered controls on $CaCO_3$ nucleation.

KEYWORDS: sulfate, $CaCO_3$, vaterite, calcite, heterogeneous nucleation, interfacial energy

Synopsis

Sulfate non-linearly increases the effective interfacial energy of $CaCO_3$, inhibiting its nucleation kinetics during scaling formation and geologic carbon sequestration.

Introduction

Calcium carbonate's ($CaCO_3$) nucleation and crystallization processes (e.g., growth and Ostwald ripening) are important because $CaCO_3$ is widely distributed in geological formations, including sediments, soils,[1, 2] and biological systems, such as biominerals in marine organisms.[3, 4] In addition, $CaCO_3$ scaling affects the efficiency of many engineered systems, such as CO_2-related subsurface projects, oil and gas recovery, geothermal projects, and water treatment and distribution systems.[5-7] Sulfate, a major environmental anion, is abundant in both seawater (28 mM) and subsurface brine (1–50 mM), where $CaCO_3$ frequently forms.[8, 9] Also, sulfate ions coexist with $CaCO_3$. For example, sulfate has been found in biominerals, such as corals and brachiopod shells,[10, 11] in amounts reaching 2%. In desalination facilities and oil field pipelines, sulfate ions can lead to scale composed of coexisting $CaCO_3$ and $CaSO_4$.[12, 13] In wellbore casings, sulfate can mitigate CO_2 attack on cement, enhancing cement's mechanical properties by hindering the rates of $CaCO_3$ formation and dissolution in the cement matrix during its deterioration.[14]

The ubiquitous coexistence of sulfate with $CaCO_3$ has attracted attention to how it affects the formation and subsequent crystallization of $CaCO_3$. A previous study found that sulfate can adsorb on growing vaterite spherulites, decreasing their growth rate.[15] In addition, a molecular dynamics study found that sulfate can enhance the stability and persistence of vaterite at micron scale.[16] However, it is still unclear how sulfate affects polymorphism at the $CaCO_3$ nucleation stage or at later crystallization stages at nanoscale. Furthermore, although sulfate's inhibition of $CaCO_3$ formation is widely acknowledged,[15-20] previous studies have mostly focused on $CaCO_3$ formation as a whole process, where mineral nucleation, mineral growth, and phase transformation are convoluted rather than discrete steps. However, the nucleation step should be clearly understood as an explicit step, because the nucleation stage generates a large amount of reactive

surface area that is indispensable in following steps, and it can control the location of the $CaCO_3$ formation.[21, 22] Furthermore, although sulfate adsorption and incorporation on/into $CaCO_3$ have been reported,[14-16] we have a surprisingly sparse understanding of sulfate's effect on $CaCO_3$ heterogeneous nucleation as an explicit step differentiated from its growth, which makes it hard to fully understand how sulfate changes $CaCO_3$ formation in natural and engineered systems.

In addition to scant experimental observations of sulfate-$CaCO_3$ interactions at the nucleation stage, a quantitative relationship between additive concentrations and the important thermodynamic parameters determining nucleation is also lacking. For this reason, one cannot directly use the knowledge of fluid-$CaCO_3$ interactions to more accurately design the $CaCO_3$ nucleation process. One of the most important thermodynamic parameters for $CaCO_3$ heterogeneous nucleation is the effective interfacial energy, α' (mJ/m^2), which can directly determine the nucleation barrier (ΔG^* (J/mol) as shown in Equation 1:[23]

$$\Delta G^* = \frac{16\pi v_m^2 \alpha'^3}{3k_B^2 T^2 \sigma^2}, \quad (1)$$

where k_B is the Boltzmann constant (J/K), T is the temperature (K), v_m is the volume per molecule of the nucleating phase, and σ is the supersaturation ($\ln(IAP/K_{sp})$). IAP is the ion activity product $(Ca^{2+})(CO_3^{2-})$, and K_{sp} is the equilibrium solubility product of $CaCO_3$. A small change in the effective interfacial energy results in a several orders of magnitude difference in nucleation rates, which depend exponentially on the nucleation barrier (ΔG^*). When particles are extremely small, the interfacial energy contribution can make a metastable phase polymorph more stable than the known thermodynamically stable phase.[24] In the case of $CaCO_3$, a density-functional theory study suggested that Mg^{2+} can tune the interfacial energy of $CaCO_3$ to enable the nucleation of a metastable phase (aragonite) instead of calcite.[25] Therefore, effective interfacial energy change can determine the kinetics and polymorphs of $CaCO_3$ in the nucleation stage, which is critical for

67 controlling the amount and function of $CaCO_3$ materials. Still, how sulfate modifies $CaCO_3$'s
68 interfacial energy remains unclear. It is essential to understand the effects of abundant components
69 in an aqueous solution on $CaCO_3$'s nucleation to more systematically and accurately study $CaCO_3$
70 formation.[2, 25-27] Here, to illuminate the poorly defined contributions of anions in $CaCO_3$
71 heterogeneous nucleation, we explore the quantitative relationship between aqueous sulfate
72 concentrations and $CaCO_3$'s effective interfacial energy.

73 Using *in situ* X-ray scattering techniques, this work systematically investigated the effects
74 of aqueous sulfate on heterogeneous $CaCO_3$ nucleation on quartz substrates. First, compared with
75 an experiment conducted with no sulfate addition, a significantly decreased nucleation rate and
76 increased nuclei size were observed when 10 mM sulfate was added. We also found that with 1–
77 10 mM sulfate addition, vaterite is stabilized over calcite. With a modification of classical
78 nucleation theory, we revealed a non-linear relationship between the effective interfacial energies
79 of heterogeneously nucleated $CaCO_3$ on a quartz surface and the aqueous sulfate concentrations.
80 The non-linear relation unveiled here highlights the impacts of impurities on solvent–solute
81 interactions in the current nucleation model, especially for sulfate, which is a large anion. The
82 findings also have great importance for broader scientific disciplines associated with $CaCO_3$ by
83 providing much needed information for effectively managing $CaCO_3$ mineral formation (e.g.,
84 scaling in oil and gas recovery and desalination systems).

85 **Materials and Methods**

86 **Quartz substrate and solution preparation.** Quartz substrates ((100) surface roughness of < 5
87 Å, 2 inches in diameter, and 0.5 mm thick) were purchased from MTI Corporation (USA) and cut
88 into 1 cm × 1 cm × 0.5 mm square pieces for use in flow-through GISAXS/GIWAXS and AFM

experiments. Ground quartz powders were used for quantifying sulfate adsorption/incorporation in batch experimental systems. The quartz substrates were cleaned thoroughly as described in the Supporting Information (SI) text S1A. $CaCl_2$ and $NaHCO_3$/Na_2SO_4 solutions were prepared from ACS reagent grade chemicals in the concentrations listed in Table 1. Ca^{2+} concentrations were chosen based on the composition of typical subsurface formation water (0.01–0.2 M).[9] The Ca^{2+}/HCO_3^- ratio was selected to fall within the range of ratios found in formation water and seawater.[2, 9] Also, these values allowed heterogeneous nucleation to occur within the experimentally detectable windows of both GISAXS/GIWAXS and AFM within a reasonable reaction time. An additional description of solution chemistry is available in SI text S1B.

Flow-through experiments, in situ X-ray data collection, and ex situ AFM measurements. This *in situ* X-ray scattering experiments were conducted at beamline 12-ID-B at the Advanced Photon Source (Argonne National Laboratory, USA). The experimental setup is shown in Figure S1. $CaCl_2$ and $NaHCO_3$/Na_2SO_4 solutions were pumped into the reactor at a flowrate of 5.6 ml/min (the flowrate is discussed in SI text S1C) and formed $CaCO_3$ nuclei on the quartz substrate for 90 mins. A 14 keV X-ray beam (200 μm wide and 20 μm high), incident on the quartz substrate at an angle of 0.11° (which gave a reflectivity of 98.8% from quartz), was scattered by newly formed nanoparticles on the substrate. Duplicate GISAXS experiments have been conducted. The 2D GISAXS scattering pattern collected by a Pilatus 2M detector was analyzed. In brief, the 1D scattering pattern from the particles (q range 0.005–0.12 $Å^{-1}$) on the quartz surface was obtained from in-plane cutting along the Yoneda wing in the same way as described in our previous studies.[26-36] Nucleus sizes and nucleation rates were obtained from the 1D scattering pattern by fitting the scattering pattern (Equation S1 in SI) and calculating the invariant value. After 90 mins of GISAXS data collection, the nucleus phases were obtained by analyzing the 2D scattering

pattern (GIWAXS) collected by a Perkin Elmer 4k × 4k detector. Detailed X-ray scattering data collection and analysis are available in SI text S1C and S1D. To quantify the nucleus heights and particle densities on substrate, the reacted quartz samples were also measured complementarily by AFM (details are available in SI text S1E).

Batch experiments and ex situ analyses. Triplicate batch experiments were conducted to synthesize heterogeneously nucleated $CaCO_3$ on quartz powders that were then used to investigate $CaCO_3$–sulfate–quartz interactions. For each experiment, 50 ml of $CaCl_2$ solution and 50 ml of $NaHCO_3/Na_2SO_4$ solution were added to a 100 ml bottle containing 0.05 g of clean quartz powder. After a 90 mins $CaCO_3$ heterogeneous nucleation experiment, solutions were vacuum filtered to collect the nuclei formed on the quartz powders. For the sulfate adsorption experiments, Na_2SO_4 solutions (pH = 7.9) were added to freshly synthesized heterogeneous nuclei. After a 90 mins sulfate adsorption experiment, the nuclei were collected by vacuum filtration. To identify the $CaCO_3$ phase on quartz powders, ATR-FTIR (Thermo Scientific Nicolet iS10 spectrometer) was used. To measure the extents of Ca^{2+} and SO_4^{2-} in $CaCO_3$ nuclei, the obtained nuclei were dissolved by 1% HCl. Sulfate concentrations were measured by IC (Thermo Scientific Dionex ICS-1600), and calcium concentrations were measured by ICP-OES (PerkinElmer Optima 7300 DV). Detailed descriptions are available in SI text S1F and S1G.

Results and Discussion

Nucleation rates and nucleus sizes of $CaCO_3$ nanoparticles on quartz

Using *in situ* GISAXS experiments, we observed the heterogeneous nucleation of $CaCO_3$ on the (100) surface of a quartz substrate in real-time, as successfully demonstrated in our previous work.[26-35, 37] The continuous increase of GISAXS intensity, *I(q)*, over a *q* range of 0.005–0.12 $Å^{-1}$

over time suggested new nanoparticle formation. Figure 1 shows representative *I(q)* vs. q values from GISAXS 1-D plots under different sulfate concentrations, after the background intensity from water was subtracted. With the assumption of in-plane spherical particle formation and the Schultz size distribution, using Equation S1 we fitted the GISAXS pattern to obtain the in-plane radius of gyration (R_g) of the nuclei.[26, 27, 30] Because there is no discernable scattering from the start of the experiments until we detected the first observable particles, it is assumed that the first observable particle size was the critical nucleus radius (r_c).[26] For 0, 1, 5, and 10 mM sulfate, the first observable R_g were 4.7 ± 0.3 nm, 5.8 ± 0.4 nm, 6.9 ± 0.5 nm, and 10.9 ± 0.6 nm, respectively. Notably, the r_c values for systems with 5 mM sulfate addition exhibited a 50% increase, and they showed an even higher increase (120%) at 10 mM sulfate than at 0 mM sulfate. Meanwhile, within our 90 mins reaction time, the fitted particle size did not significantly increase under our tested conditions, which indicated that the reaction systems were nucleation-dominated, and that particle growth was not significant.

Nucleation rates were calculated from invariant values and fitted particle numbers (Figure 2). The invariant value, $Q = \frac{1}{2\pi^2}\int I(q)q^2dq$, indicates total particle scattering and is proportional to the total particle volumes for each tested condition.[28] Thus, when the system is nucleation-dominated, the invariant values can represent total particle numbers.[28, 31] After the induction time (the stagnant period of invariant values in Figure 2), the nucleation rate was obtained from a linear regression of the linear region of the invariant versus time (before the linear region, the relation between the invariant and reaction time shows a convex curve).[27] In the same way, linear regression analyses of the fitted particle numbers (*N* from Equation S1 in SI) with respect to reaction time also provided the nucleation rates. The calculated invariant values and fitted particle numbers are plotted in Figure 2, which shows that the nucleation rates from both methods were

consistent: The nucleation rate decreases with the addition of sulfate. From the fitted particle numbers, compared with 0 mM sulfate condition, the nucleation rates decrease by 59%, 80%, and 88% in the 1, 5, and 10 mM sulfate systems, respectively. In previous research by Bots et al., adding 50 mM sulfate decreased the overall rate (nucleation + growth rate) of $CaCO_3$ by 81%.[15] Considering that we found an 88% rate decrease at just the nucleation stage, and at a rather lower sulfate concentration of only 10 mM, it is clear that the nucleation stage is critical in inhibiting $CaCO_3$ formation in the presence of sulfate.

The newly formed particle sizes and particle densities (#/μm^2) of $CaCO_3$ on quartz were also analyzed by *ex situ* atomic force microscopy (AFM) after 90 mins of reaction (Figure S4-5). Based on six selected 2 μm × 2 μm areas from three replicate samples, there were 54 ± 12 #/μm^2 nuclei on quartz with 10 mM sulfate, versus 302 ± 43 #/μm^2 without sulfate, indicating a lower heterogeneous nucleation rate. Moreover, at 1, 5, and 10 mM sulfate concentrations, the average heights of 100 particles nucleated on quartz substrates increased from 1.3 ± 0.3 nm (0 mM sulfate) to 1.7 ± 0.6 nm, 2.1 ± 0.4 nm, and 2.6 ± 0.8 nm, respectively. These observed trends of particle sizes and densities with respect to sulfate concentrations were consistent with those from GISAXS.

Solid phase determination of $CaCO_3$ nanoparticles and evaluation of $CaCO_3$–sulfate–quartz interactions

To confirm the solid phase of heterogeneously nucleated $CaCO_3$ nanoparticles on quartz, we conducted GIWAXS measurements very shortly after the 90 mins GISAXS experiments. The results are shown in Figure 3a. To exclude homogeneously nucleated $CaCO_3$ particles that could have collected on substrates by collision and gravitational settlement during the GISAXS experiments, we rinsed the reacted quartz with anhydrous ethanol to remove all physically

accumulated particles,[26, 27, 30] and then made GIWAXS measurements within 5 mins. Furthermore, we designed our experimental solutions to be undersaturated with respect to gypsum ($CaSO_4 \cdot 2H_2O$), as shown in Table 1. As expected, major peaks of gypsum and anhydrite, such as those at 11.67° and 31.34°, were not observable in the GIWAXS patterns (Figure 3a).[38, 39] The peak at 20.87° was attributed to the (100) quartz substrate instead of gypsum, because even the 0 mM sulfate condition had this peak.[40] Regarding the $CaCO_3$'s phase, for all conditions, peaks were observed at 24.89°, 27.05° and 32.74°, indicating the presence of vaterite.[41] Furthermore, only the 0 mM sulfate condition showed additional characteristic peaks of calcite (stars in Figure 3a), the most thermodynamically stable $CaCO_3$ polymorph, at 29.3° and 39.5°.[42] Aragonite was not observed in any conditions. Because a phase transformation from vaterite to calcite is commonly observed in impurity-free solutions,[43] we suggest that the presence of sulfate hinders the crystallization of $CaCO_3$ into its most thermodynamically stable phase. Though amorphous calcium carbonate (ACC) may form as a metastable phase during the nucleation process, we did not observe ACC after 90 mins of reaction, based on the fact that there is no broad peak around 30° and 45°.[43]

Previous studies reported that both sulfate incorporation into the $CaCO_3$ lattice and sulfate adsorption on Ca sites could inhibit $CaCO_3$ crystallization.[15, 16, 20] To examine the main contributor(s) to altered $CaCO_3$ phase transformation, we quantified the sulfate amounts in heterogeneously formed $CaCO_3$ nuclei by conducting batch experiments using quartz powders. Note that the reaction time in batch experiments was exactly the same as in our GISAXS experiment, so nucleation dominated the reaction system and there was no mineral growth. The phase of heterogeneously nucleated $CaCO_3$ on quartz powder was identified by FTIR. The infrared spectra of the samples (Figure 3b) showed peaks characteristic of both carbonate (1,425 cm^{-1} (ν_3),

863 cm^{-1} (ν_2), and 747 cm^{-1} (ν_4)) and silica (1,038 cm^{-1}).[44] The presence of carbonate bands (ν_4) at 747 cm^{-1} suggests that the major $CaCO_3$ phase was vaterite.[44] Moreover, at the C–O stretching mode (ν_3) near 1450 cm^{-1}, the 0 mM sulfate condition showed a sharper peak than those in the other sulfate-containing systems, while both the 1 mM and 10 mM sulfate conditions exhibited broader and split peaks. Calcite exhibits one sharp peak at ν_3, while vaterite exhibits split peaks at ν_3,[4, 45-47] suggesting that vaterite has partially transformed to calcite in the 0 mM sulfate condition. The heterogeneously nucleated $CaCO_3$ on quartz powder showed similar $CaCO_3$ phases under different sulfate concentrations to those we observed in GIWAXS.

To quantify the Ca^{2+} and SO_4^{2-} contents in the nuclei, $CaCO_3$ nanoparticles nucleated on quartz powders were dissolved and then measured by inductively coupled plasma optical emission spectrometry (ICP-OES) and ion chromatography (IC), respectively. Nuclei formed at 1, 5, and 10 mM sulfate concentrations exhibited SO_4^{2-}/Ca^{2+} molar ratios of $2.7 \pm 0.4 \times 10^{-3}$, $5.5 \pm 0.5 \times 10^{-3}$, and $9.1 \pm 1.4 \times 10^{-3}$ (shown as **Total sulfate** in Table 2). Assuming the total sulfate could be either incorporated or adsorbed, if we determine the adsorbed sulfate amounts, we can then calculate the incorporated amounts by subtracting those values from the total extents. To test the calculated amounts, we first synthesized heterogeneously nucleated $CaCO_3$ on quartz powders in the absence of sulfate. Then, those nuclei (together with quartz powders) were placed in 1, 5, and 10 mM sulfate solutions at pH = 7.9 to adsorb sulfate ions on $CaCO_3$ surfaces. We quantified the **adsorbed sulfate** (shown in SO_4^{2-}/Ca^{2+} molar ratios) from these $CaCO_3$ nuclei after a 90 mins sulfate adsorption experiment and then calculated the **incorporated sulfate** (shown in SO_4^{2-}/Ca^{2+} molar ratios) by subtracting the **adsorbed sulfate** from the **total sulfate**. For all conditions, sulfate incorporation is greatly dominant over sulfate adsorption (Table 2).

Surface potentials can explain the lesser extent of sulfate adsorption compared with sulfate incorporation (Figure S6). In DI water and SO_4^{2-} solutions, the zeta potentials of quartz powders were between -25 to -27mV (Figure S6a), suggesting that Ca^{2+} could be preferentially adsorbed on quartz powders. Then, at the early stage of nucleation, CO_3^{2-} would react with Ca^{2+} to nucleate ACC or the crystalline phase and SO_4^{2-} would incorporate into nuclei. Because the zeta potentials of $CaCO_3$ are positive,[27] during $CaCO_3$ nucleation, the net zeta potentials of quartz powders with $CaCO_3$ nuclei become less negative (-12 mV) (Figure S6b). However, after $CaCO_3$ forms on quartz, the resulting surface is still negative and can repel the negatively charged sulfate ions and make the sulfate adsorption extent become extreme low. To be noted, no matter whether the nuclei phase is ACC or vaterite or calcite, this electrostatic repulsion would inhibit sulfate adsorption. It is unclear that if crystalline $CaCO_3$ would have less interactions with sulfate.

Based on previous works, the incorporated sulfate could inhibit the vaterite-to-calcite phase transformation at micron scale. Navrotsky et al., found that calcite has a lower free energy than vaterite by ~3 kJ/mol.[48] However, a molecular simulation by Fernández-Díaz et al. found that, when the sulfate incorporation extent was less than 2%, the free energy of vaterite decreased, and in contrast, the free energy of calcite increased.[16] If we consider these aspects, a 0.9% sulfate incorporation in our study would decrease vaterite's free energy by ~2 kJ/mol and increase calcite's free energy by ~1.8 kJ/mol. Their free energy changes are illustrated in Figure 3c. Thus, when sulfate is incorporated into $CaCO_3$ systems, the phase transformation energy from sulfate-incorporated-vaterite to sulfate-incorporated-calcite becomes positive, preventing the phase transformation of nuclei formed in the presence of sulfate. Supersaturation is quantified by the ratio between *IAP and* K_{sp}. As shown in Table 1, the calculated supersaturations (IAP/K_{sp}) were the same for all four conditions in our study, based on the assumption in the Geochemist's

Workbench (GWB) model calculations that K_{sp} was not changed by sulfate. Hence, sulfate did not significantly affect the *IAP* of $CaCO_3$ in our experimental systems. Next, we considered whether the incorporation of sulfate could affect nuclei's K_{sp} and result in significantly inhibited nucleation kinetics. As our GIWAXS data showed, the nuclei formed in the 10 mM sulfate condition were vaterite. Moreover, 0.9% sulfate incorporation would decrease vaterite's bulk free energy by 2 kJ/mol, based on the molecular simulation work by Fernández-Díaz et al. (2010).[9] Considering that sulfate-free-vaterite has a bulk free energy of -45.5 kJ/mol,[21] the bulk free energy of $CaCO_3$ formed in the 10 mM sulfate condition can be estimated as -47.5 kJ/mol. For the 0 mM sulfate condition, the nuclei were a combination of calcite and vaterite in our experimental systems. Based on the ratios of peak intensities at 27.0° (the highest intensity peak for vaterite) and 29.4°(the highest intensity peak for calcite) in the GIWAXS results (Figure 3a), we estimated the amount ratio for vaterite:calcite to be 55:45. Using this ratio, we calculated the bulk free energy of nuclei in the 0 mM sulfate condition as $0.55 \times (-45.5) + 0.45 \times (-48.4) = -46.8$ kJ/mol. Through this calculation, we found that the bulk free energy of nuclei formed in the 10 mM sulfate system was slightly lower than that in 0 mM sulfate system, by 0.7 kJ/mol. Furthermore, a lower bulk free energy indicated a smaller K_{sp}. Considering that *IAP* was the same for all conditions, a smaller K_{sp} would result in a larger supersaturation. If supersaturation were the dominant thermodynamic parameter controlling the nucleation kinetics, the nucleation rate should be faster in the 10 mM sulfate condition. However, our experimental observation showed an opposite trend, which suggests that another thermodynamic parameter, the effective interfacial energy, may dominate the nucleation kinetics.

The effective interfacial energy of $CaCO_3$ nuclei increases as sulfate incorporates

As mentioned, the effective interfacial energy of $CaCO_3$ nuclei (α') is critical for determining the heterogeneous nucleation kinetics, but no prior study has shown a quantitative relationship between additive concentrations and α' evolution. In the case of sulfate, our results suggests that α' change is more impactful than supersaturation change, and a quantitative relationship between sulfate concentration and α' is critical for designing the nucleation rates of engineered materials. To mathematically quantify how much the sulfate impurity can change the $CaCO_3$ effective interfacial energy, we devised a new term, called an interfacial energy factor (k), which describes the relationship between the interfacial energies of $CaCO_3$ formed with sulfate addition ($\alpha'_{sulfate}$) and that of $CaCO_3$ formed without sulfate addition (α'_{0mM}): $k = \alpha'_{sulfate}/\alpha'_{0mM}$. From the GISAXS measurements, we obtained heterogeneous $CaCO_3$ nucleation rates with sulfate addition ($J_{sulfate}$) and without sulfate addition (J_{0mM}). Using the nucleation rate ratio ($J_{sulfate}/J_{0mM}$), we could quantify the interfacial energy factor (k) as Equation 2 shows (A detailed derivation is in SI text S2A):

$$k = \sqrt[3]{-\frac{3k_B^3T^3\sigma^2 ln\frac{J_{sulfate}}{J_{0mM}}}{16\pi v_m^2(\alpha'_{0mM})^3} + 1}. \quad (2)$$

In our experimental systems, different sulfate concentrations resulted in different nucleus phases containing various vaterite and calcite combinations. Hence, by using either the parameters from vaterite or those from calcite, as shown in Figure 4a and 4c we could obtain the lower limit (blue line) and the upper limit (purple line) for our interfacial energy factor (k) as the sulfate concentrations/incorporated sulfate extents increase. Shown in Figure 4a, as sulfate concentrations increase, the effective interfacial energies of nuclei constantly increase in a non-linear way.

The non-linear evolution of $CaCO_3$ effective interfacial energies with increased sulfate concentrations poses difficulties in precisely predicting $CaCO_3$ nucleation. Accordingly, we investigated the relationship between aqueous sulfate concentrations and incorporated sulfate

extents in $CaCO_3$ nuclei. As Figure 4b shows, with the increasing sulfate concentrations, the incorporated sulfate extent at higher concentrations (1–10 mM) increases less steeply than at lower concentrations (0–1 mM). This behavior is similar to a previously reported decreased tendency for Mg^{2+} incorporation into $CaCO_3$ at higher concentrations.[49] Although that report did not confirm the non-linear relationship between effective interfacial energies and aqueous Mg^{2+} concentrations, the relationship can be non-linear, as we found here.

We then investigated the relationship between the interfacial energy factors (*k*) and incorporated sulfate extents and found the trend was still non-linear. In our study, sulfate serves as an impurity in both the aqueous solution and $CaCO_3$ nuclei, increasing the effective interfacial energy of $CaCO_3$. Thus, there is a higher barrier for generating new $CaCO_3$ solid from a supersaturated solution. Although a direct comparison cannot be made, ice nucleation exhibits a similar behavior in the presence of impurities. With the increasing concentration, impurities non-linearly depress the freezing point, raising the nucleation barrier for ice in a supercooled solution,[50] due to solute–solute and solute–solvent interactions.[51] In a similar way, solute–solvent interaction could cause the non-linear evolution of the effective interfacial energy of $CaCO_3$ with respect to the extents of incorporated sulfate.

In addition, in $CaCO_3$ nucleation, amorphous calcium carbonate (ACC) has been reported as a metastable phase existing before the crystalline phase[52-54]. Although we did not detect ACC after 90 minutes reaction, it could exist in the early moments. Therefore, we also calculated the effective interfacial energy of ACC (see SI text S2B). Although ACC develops only 20–30% of the crystalline phase's effective interfacial energy[52], our results still showed a non-linear evolution trend (Figure S8), which strongly suggests that sulfate played a significant role in ACC formation as well.

Next, previous $CaCO_3$ nucleation studies have found the formation of stable clusters as intermediates before critical nuclei formation[55-57], and we were curious about how sulfate can affect these prenucleation clusters. Building on more and more experimental and modeling proofs of the existence of prenucleation clusters, a recent effort has improved the expression of the nucleation energy barrier (ΔG_c) by incorporating an excess energy term to reflect the effects of prenucleation clusters.[58]. Their revised model is formulated in Equation 3:

$$\Delta G_c = \frac{16\pi v_m^2 \alpha'^3}{3k_B^2 T^2 \sigma^2}\left(1 + \frac{4v_m \alpha_{cluster}}{r_{cluster} kT\sigma}\right)^{-2}, \quad (3)$$

In this revised model, in addition to the parameters in classical nucleation theory, the interfacial energy of clusters ($\alpha_{cluster}$) and the cluster radius ($r_{cluster}$) were included. Given the evidence that $CaCO_3$ prenucleation cluster sizes ranges from 0.9 to 4 nm[56], while the length of $CaSO_4$ prenucleation clusters is 2.8 nm[59], no clear sulfate-dependent $r_{cluster}$ changes can be expected. For $CaCO_3$ heterogeneous nucleation to occur in the presence of sulfate, both HCO_3^- and additive SO_4^{2-} need to be dehydrated and bound with Ca^{2+}. Because the hydration energy for SO_4^{2-} (-1,080 kJ/mol) is much lower than that for HCO_3^- (-335 kJ/mol)[60] we postulate that when more sulfate is incorporated into the $CaCO_3$ cluster, clusters may interact more strongly with solvent, changing the value of $\alpha_{cluster}$ and eventually causing a non-linear interfacial energy evolution. Unfortunately, no experimental or modeling work has reported a value for $\alpha_{cluster}$, let alone provided a quantitative relationship between $\alpha_{cluster}$ and additive concentrations. Here, as a brief summary, sulfate incorporated into the nucleation clusters and caused stronger interactions with water, which in turn caused the effective interfacial energy of the ACC and crystalline phases to evolve non-linearly. Once a better way to quantitatively measure the energies of nucleation clusters has been developed, we expect that our current quantitative model can be further improved.

Environmental Implications

This study shows that sulfate can both thermodynamically and kinetically affect heterogeneous nucleation of $CaCO_3$ on the (100) surface of quartz. With the increased sulfate concentrations, the nucleation rates of $CaCO_3$ decreased and their nucleus sizes increased. These newly formed $CaCO_3$ particles in sulfate systems were identified as vaterite. Within the 1–10 mM sulfate concentrations in our study, sulfate was incorporated much more than that was adsorbed on $CaCO_3$. We found that the heterogeneous $CaCO_3$ nucleation is more sensitive at lower sulfate concentrations (< 1 mM), and the increment of the effective interfacial energy increase becomes less at high sulfate concentrations. Hence, effective interfacial energies and sulfate concentrations exhibit a non-linear relationship.

Heterogeneous nucleation of $CaCO_3$ is important in biominerals formation in natural environments. Previous studies have mostly focused on the effects of cations, macromolecular proteins, and organic matrixes on $CaCO_3$ nucleation.[48, 61] For example, interfacial energy of different polysaccharides regulates the $CaCO_3$ nucleation kinetics.[61] Moreover, a molecular simulation work revealed that that 1% Mg incorporation increases the surface energy of calcite from 0.21 to 0.23 J/m^2, a 9.5% increase.[25] In our experimental work, however, a sulfate incorporation of only 0.9% caused a 11.7%–15.4% increase in the interfacial energy of $CaCO_3$ nanoparticles on quartz, which is higher than the Mg incorporation reported. We suggest that, as a larger ion, when sulfate (with an ionic radius of 0.242 nm)[16] substitutes for carbonate within $CaCO_3$, it can cause more severe lattice distortion than the incorporation of Mg (with an ionic radius 0.130 nm).[16] Our previous work observed faster heterogeneous $CaCO_3$ nucleation at higher Cl^- concentrations because higher ionic strengths could decrease the interfacial energy and kinetic

358 factor of $CaCO_3$.[27] Our study here further highlights the underestimated impacts of anions on
359 $CaCO_3$ nucleation especially when they can incorporate into nuclei.

360 Heterogeneous nucleation of $CaCO_3$ is also critical for effective management of water-
361 energy engineered systems *via* mineral fouling in membrane process and mineral carbonation
362 during geologic carbon sequestration. For the first time, we experimentally determined the
363 relationship between the effective interfacial energies of $CaCO_3$ and the sulfate concentrations in
364 solutions. Our improved understanding of nucleation rates and effective interfacial energy
365 information can be directly incorporated into the reactive transport modeling to improve the
366 prediction of mineral scaling on membrane and $CaCO_3$ formation in sediments from two aspects.
367 One is that we can better predict the distribution and amounts of $CaCO_3$. A quantitative description
368 of sulfate-inhibited nucleation can help us to precisely calculate initial reactive surface area,
369 distribution, and amount of $CaCO_3$, which current models without considering nucleation are less
370 capable to predict. Another is that we can avoid an overestimation of the change of $CaCO_3$
371 nucleation kinetics at high sulfate concentrations because our study suggests that further increasing
372 sulfate concentrations would not decrease nucleation rate significantly. These quantitative
373 descriptions provided in this study can help us to manage scale formation in desalination and oil
374 field pipes. They can also improve the mineral carbonation efficiency and to understand the fate
375 and transport of injected CO_2 during geologic CO_2 sequestration.

Acknowledgments

This work is supported by the Center for Nanoscale Control of Geologic CO_2, an Energy Frontier Research Center funded by the U.S. Department of Energy, Office of Science, Office of Basic Energy Sciences under Award Number DE-AC02-05CH11231 and Washington University's Consortium for Clean Coal Utilization. The Nano Research Facility at Washington University in St. Louis provided their facilities for the experiments. Use of the Advanced Photon Source (sectors 12-ID-B) at Argonne National Laboratory was supported by the U.S. Department of Energy, Office of Science, Office of Basic Energy Sciences, under Contract No. DE-AC02-06CH11357. We thank Prof. J. Ballard for carefully reviewing our manuscript.

Supporting Information

Supporting description of materials and methods (S1); Modified classical nucleation theory and related discussions (S2); Schematic diagram and picture of experimental setup for in situ GISAXS and GIWAXS experiments (Figure S1); Replicate GISAXS patterns for four different sulfate concentrations (Figure S2); Invariant values and fitted particle numbers from replicate GISAXS experiment (Figure S3); Representative 2 μm × 2 μm AFM images of quartz substrates after 90 mins of reaction at different sulfate concentrations (Figure S4); Representative AFM height mode images (Figure S5); Surface charge measurements of particles in batch experiments (Figure S6); Effects of different $CaCO_3$ polymorphs on the evolution of their interfacial energy factor k values (Figure S7); Effects of sulfate on the evolution of effective interfacial energy of amorphous calcium carbonate (Figure S8).

References

1. Feely, R. A.; Sabine, C. L.; Lee, K.; Berelson, W.; Kleypas, J.; Fabry, V. J.; Millero, F. J., Impact of anthropogenic CO_2 on the $CaCO_3$ system in the oceans. *Science* **2004,** *305*, (5682), 362–366.
2. Morse, J. W.; Arvidson, R. S.; Lüttge, A., Calcium carbonate formation and dissolution. *Chem. Rev.* **2007,** *107*, (2), 342–381.
3. Mann, S., Molecular recognition in biomineralization. *Nature* **1988,** *332*, (6160), 119.
4. Addadi, L.; Raz, S.; Weiner, S., Taking advantage of disorder: amorphous calcium carbonate and its roles in biomineralization. *Adv. Mater.* **2003,** *15*, (12), 959–970.
5. Min, Y.; Li, Q.; Voltolini, M.; Kneafsey, T.; Jun, Y.-S., Wollastonite carbonation in water-bearing supercritical CO_2: Effects of particle size. *Environ. Sci. Technol.* **2017,** *51*, (21), 13044–13053.
6. Helgeson, H. C.; Knox, A. M.; Owens, C. E.; Shock, E. L., Petroleum, oil field waters, and authigenic mineral assemblages Are they in metastable equilibrium in hydrocarbon reservoirs. *Geochim. Cosmochim. Acta* **1993,** *57*, (14), 3295–3339.
7. Tzotzi, C.; Pahiadaki, T.; Yiantsios, S.; Karabelas, A.; Andritsos, N., A study of $CaCO_3$ scale formation and inhibition in RO and NF membrane processes. *J. Membr. Sci.* **2007,** *296*, (1-2), 171–184.
8. Canfield, D. E.; Farquhar, J., Animal evolution, bioturbation, and the sulfate concentration of the oceans. *Proc Natl Acad Sci USA* **2009,** *106*, (20), 8123–8127.
9. Kharaka, Y. K.; Hanor, J., Deep fluids in the continents: I. Sedimentary basins. *Treatise Geochem.* **2003,** *5*, 605.
10. Balthasar, U.; Cusack, M., Aragonite-calcite seas—Quantifying the gray area. *Geology* **2015,** *43*, (2), 99–102.
11. Cusack, M.; Dauphin, Y.; Cuif, J.-P.; Salomé, M.; Freer, A.; Yin, H., Micro-XANES mapping of sulphur and its association with magnesium and phosphorus in the shell of the brachiopod, Terebratulina retusa. *Chem. Geol.* **2008,** *253*, (3-4), 172–179.
12. Moghadasi, J.; Jamialahmadi, M.; Müller-Steinhagen, H.; Sharif, A.; Ghalambor, A.; Izadpanah, M.; Motaie, E. In *Scale formation in Iranian oil reservoir and production equipment during water injection*, International Symposium on Oilfield Scale, 2003; Society of Petroleum Engineers: 2003.
13. Ray, J. R.; Wong, W.; Jun, Y.-S., Antiscaling efficacy of $CaCO_3$ and $CaSO_4$ on polyethylene glycol (PEG)-modified reverse osmosis membranes in the presence of humic acid: interplay of membrane surface properties and water chemistry. *Phys. Chem. Chem. Phys.* **2017,** *19*, (7), 5647–5657.
14. Li, Q.; Lim, Y. M.; Jun, Y.-S., Effects of sulfate during CO_2 attack on Portland cement and their impacts on mechanical properties under geologic CO_2 sequestration conditions. *Environ. Sci. Technol.* **2015,** *49*, (11), 7032–7041.
15. Bots, P.; Benning, L. G.; Rodriguez-Blanco, J.-D.; Roncal-Herrero, T.; Shaw, S., Mechanistic insights into the crystallization of amorphous calcium carbonate (ACC). *Cryst. Growth Des.* **2012,** *12*, (7), 3806-3814.
16. Fernández-Díaz, L.; Fernández-González, Á.; Prieto, M., The role of sulfate groups in controlling $CaCO_3$ polymorphism. *Geochim. Cosmochim. Acta* **2010,** *74*, (21), 6064–6076.
17. Walter, L. M., Relative efficiency of carbonate dissolution and precipitation during diagenesis: a progress report on the role of solution chemistry. **1986**.

18. Reddy, M.; Nancollas, G., The crystallization of calcium carbonate: IV. The effect of magnesium, strontium and sulfate ions. *J. Cryst. Growth* **1976,** *35*, (1), 33–38.
19. Sibley, D. F.; Nordeng, S. H.; Borkowski, M. L., Dolomitization kinetics of hydrothermal bombs and natural settings. *J. Sediment. Res.* **1994,** *64*, (3a), 630–637.
20. Tang, Y.; Zhang, F.; Cao, Z.; Jing, W.; Chen, Y., Crystallization of $CaCO_3$ in the presence of sulfate and additives: Experimental and molecular dynamics simulation studies. *J. Colloid Interface Sci.* **2012,** *377*, (1), 430–437.
21. Li, Q.; Steefel, C. I.; Jun, Y.-S., Incorporating nanoscale effects into a continuum-scale reactive transport model for CO_2-deteriorated cement. *Environ. Sci. Technol.* **2017,** *51*, (18), 10861–10871.
22. Steefel, C. I.; Van Cappellen, P., A new kinetic approach to modeling water-rock interaction: The role of nucleation, precursors, and Ostwald ripening. *Geochim. Cosmochim. Acta* **1990,** *54*, (10), 2657–2677.
23. De Yoreo, J. J.; Vekilov, P. G., Principles of crystal nucleation and growth. *Rev. Mineral. Geochem.* **2003,** *54*, (1), 57–93.
24. Navrotsky, A., Nanoscale effects on thermodynamics and phase equilibria in oxide systems. *ChemPhysChem* **2011,** *12*, (12), 2207–2215.
25. Sun, W.; Jayaraman, S.; Chen, W.; Persson, K. A.; Ceder, G., Nucleation of metastable aragonite $CaCO_3$ in seawater. *Proc Natl Acad Sci USA* **2015,** *112*, 3199–3204.
26. Li, Q.; Fernandez-Martinez, A.; Lee, B.; Waychunas, G. A.; Jun, Y.-S., Interfacial energies for heterogeneous nucleation of calcium carbonate on mica and quartz. *Environ. Sci. Technol.* **2014,** *48*, (10), 5745–5753.
27. Li, Q.; Jun, Y.-S., Salinity-induced reduction of interfacial energies and kinetic factors during calcium carbonate nucleation on quartz. *J. Phys. Chem. C* **2019,** *123*, 14319–14326.
28. Jun, Y.-S.; Lee, B.; Waychunas, G. A., In situ observations of nanoparticle early development kinetics at mineral−water interfaces. *Environ. Sci. Technol.* **2010,** *44*, (21), 8182–8189.
29. Jun, Y.-S.; Kim, D.; Neil, C. W., Heterogeneous nucleation and growth of nanoparticles at environmental interfaces. *Acc. Chem. Res.* **2016,** *49*, (9), 1681–1690.
30. Li, Q.; Jun, Y.-S., The apparent activation energy and pre-exponential kinetic factor for heterogeneous calcium carbonate nucleation on quartz. *Commun. Chem.* **2018,** *1*, (1), 56.
31. Fernandez-Martinez, A.; Hu, Y.; Lee, B.; Jun, Y.-S.; Waychunas, G. A., In situ determination of interfacial energies between heterogeneously nucleated $CaCO_3$ and quartz substrates: thermodynamics of CO_2 mineral trapping. *Environ. Sci. Technol.* **2012,** *47*, (1), 102–109.
32. Hu, Y.; Lee, B.; Bell, C.; Jun, Y.-S., Environmentally abundant anions influence the nucleation, growth, ostwald ripening, and aggregation of hydrous Fe(III)oxides. *Langmuir* **2012,** *28*, (20), 7737–7746.
33. Hu, Y.; Li, Q.; Lee, B.; Jun, Y.-S., Aluminum affects heterogeneous Fe(III)(hydr)oxide nucleation, growth, and ostwald ripening. *Environ. Sci. Technol.* **2014,** *48*, (1), 299–306.
34. Hu, Y.; Neil, C.; Lee, B.; Jun, Y.-S., Control of heterogeneous Fe(III)(hydr)oxide nucleation and growth by interfacial energies and local saturations. *Environ. Sci. Technol.* **2013,** *47*, (16), 9198–9206.
35. Jung, H.; Jun, Y.-S., Ionic strength-controlled Mn(hydr)oxide nanoparticle nucleation on quartz: effect of aqueous $Mn(OH)_2$. *Environ. Sci. Technol.* **2016,** *50*, (1), 105–113.

36. Jung, H.; Lee, B.; Jun, Y.-S., Structural match of heterogeneously nucleated $Mn(OH)_2$(s) nanoparticles on quartz under various pH conditions. *Langmuir* **2016,** *32*, (41), 10735–10743.
37. Neil, C. W.; Lee, B.; Jun, Y.-S., Different arsenate and phosphate incorporation effects on the nucleation and growth of iron(III)(hydr)oxides on quartz. *Environ. Sci. Technol.* **2014,** *48*, (20), 11883–11891.
38. Schofield, P. F.; Knight, K. S.; Stretton, I. C., Thermal expansion of gypsum investigated by neutron powder diffraction. *Am. Mineral.* **1996,** *81*, (7-8), 847–851.
39. Hawthorne, F.; Ferguson, R., Anhydrous sulphates; II, Refinement of the crystal structure of anhydrite. *Can. Mineral.* **1975,** *13*, (3), 289–292.
40. Smith, G. t.; Alexander, L., Refinement of the atomic parameters of α-quartz. *Acta Crystallogr.* **1963,** *16*, (6), 462–471.
41. Wang, J.; Becker, U., Structure and carbonate orientation of vaterite ($CaCO_3$). *Am. Mineral.* **2009,** *94*, (2-3), 380–386.
42. Graf, D. L., Crystallographic tables for the rhombohedral carbonates. *Am. Mineral.* **1961,** *46*, (11–12), 1283–1316.
43. Radha, A.; Forbes, T. Z.; Killian, C. E.; Gilbert, P.; Navrotsky, A., Transformation and crystallization energetics of synthetic and biogenic amorphous calcium carbonate. *Proc Natl Acad Sci USA* **2010,** *107*, 16438–16443
44. Ihli, J.; Wong, W. C.; Noel, E. H.; Kim, Y.-Y.; Kulak, A. N.; Christenson, H. K.; Duer, M. J.; Meldrum, F. C., Dehydration and crystallization of amorphous calcium carbonate in solution and in air. *Nat. Commun.* **2014,** *5*, 3169.
45. Andersen, F. A.; Brecevic, L., Infrared spectra of amorphous and crystalline calcium carbonate. *Acta Chem. Scand.* **1991,** *45*, (10), 1018–1024.
46. Politi, Y.; Arad, T.; Klein, E.; Weiner, S.; Addadi, L., Sea urchin spine calcite forms via a transient amorphous calcium carbonate phase. *Science* **2004,** *306*, (5699), 1161–1164.
47. Sato, M.; Matsuda, S., Structure of vaterite and infrared spectra. *Z. Kristallogr. Cryst. Mater.* **1969,** *129*, (5-6), 405–410.
48. Navrotsky, A., Energetic clues to pathways to biomineralization: Precursors, clusters, and nanoparticles. *Proc Natl Acad Sci USA* **2004,** *101*, (33), 12096–12101.
49. Mucci, A.; Morse, J. W., The solubility of calcite in seawater solutions of various magnesium concentration, It= 0.697 m at 25 ^{o}C and one atmosphere total pressure. *Geochim. Cosmochim. Acta* **1984,** *48*, (4), 815–822.
50. Rasmussen, D. H.; MacKenzie, A. P., Effect of solute on ice-solution interfacial free energy; calculation from measured homogeneous nucleation temperatures. In *Water structure at the water-polymer interface*, Jellinek, H. H. G., Ed. Springer: 1972; pp 126–145.
51. Fullerton, G. D.; Keener, C. R.; Cameron, I. L., Correction for solute/solvent interaction extends accurate freezing point depression theory to high concentration range. *J. Biochem. Bioph. Methods* **1994,** *29*, (3-4), 217–235.
52. Koishi, A.; Fernandez-Martinez, A.; Van Driessche, A. E.; Michot, L. J.; Pina, C. M.; Pimentel, C.; Lee, B.; Montes-Hernandez, G., Surface Wetting Controls Calcium Carbonate Crystallization Kinetics. *Chem. Mater.* **2019,** *31*, (9), 3340-3348.
53. Smeets, P. J.; Cho, K. R.; Kempen, R. G.; Sommerdijk, N. A.; De Yoreo, J. J., Calcium carbonate nucleation driven by ion binding in a biomimetic matrix revealed by in situ electron microscopy. *Nat. Mater.* **2015,** *14*, (4), 394.
54. Nielsen, M. H.; Aloni, S.; De Yoreo, J. J., In situ TEM imaging of $CaCO_3$ nucleation reveals coexistence of direct and indirect pathways. *Science* **2014,** *345*, (6201), 1158-1162.

55. Demichelis, R.; Raiteri, P.; Gale, J. D.; Quigley, D.; Gebauer, D., Stable prenucleation mineral clusters are liquid-like ionic polymers. *Nat. Commun.* **2011,** *2*, (1), 1-8.
56. Gebauer, D.; Völkel, A.; Cölfen, H., Stable prenucleation calcium carbonate clusters. *Science* **2008,** *322*, (5909), 1819-1822.
57. Pouget, E. M.; Bomans, P. H.; Goos, J. A.; Frederik, P. M.; Sommerdijk, N. A., The initial stages of template-controlled $CaCO_3$ formation revealed by cryo-TEM. *Science* **2009,** *323*, (5920), 1455-1458.
58. Habraken, W. J.; Tao, J.; Brylka, L. J.; Friedrich, H.; Bertinetti, L.; Schenk, A. S.; Verch, A.; Dmitrovic, V.; Bomans, P. H.; Frederik, P. M., Ion-association complexes unite classical and non-classical theories for the biomimetic nucleation of calcium phosphate. *Nat. Commun.* **2013,** *4*, (1), 1-12.
59. Stawski, T. M.; Van Driessche, A. E.; Ossorio, M.; Rodriguez-Blanco, J. D.; Besselink, R.; Benning, L. G., Formation of calcium sulfate through the aggregation of sub-3 nanometre primary species. *Nat. Commun.* **2016,** *7*, (1), 1-9.
60. Marcus, Y., Thermodynamics of solvation of ions. Part 5.—Gibbs free energy of hydration at 298.15 K. *J. Chem. Soc., Faraday Trans.* **1991,** *87*, (18), 2995–2999.
61. Giuffre, A. J.; Hamm, L. M.; Han, N.; De Yoreo, J. J.; Dove, P. M., Polysaccharide chemistry regulates kinetics of calcite nucleation through competition of interfacial energies. *Proc Natl Acad Sci USA* **2013,** *110*, (23), 9261–9266.

552 **Table 1**. Experimental conditions in this study. Supersaturation (σ) is defined as ln(IAP/K_{sp}), where
553 *IAP* is the ion activity product $(Ca^{2+})(CO_3^{2-})$, and K_{sp} is the solubility product of the minerals,
554 written as a subscript of σ. Values of σ and pH were calculated by Geochemist's Workbench (GWB,
555 Release 8.0, RockWare, Inc.) using the thermo_minteq database. The Ca^{2+}/HCO_3^- ratio is fixed at
556 5. To strictly control the $\sigma_{calcite}$, the calcium concentrations are different for conditions 1 and 2.
557 Ionic strengths are controlled at 0.15 M because it can affect the heterogeneous $CaCO_3$ kinetics.[27]

Condition	$CaCl_2$ (mM)	$NaHCO_3$ (mM)	NaCl (mM)	Na_2SO_4 (mM)	pH	Ionic strength (M)	$\sigma_{calcite}$	$\sigma_{vaterite}$	σ_{gypsum}
1	36.5	7.3	27	10	7.91	0.15	3.97	2.67	-0.32
2	36	7.2	38	5	7.91	0.15	3.97	2.67	-1.00
3	35	7	43	1	7.91	0.15	3.97	2.67	-2.59
4	35	7	47	0	7.91	0.15	3.97	2.67	-

558 **Table 2**. Total sulfate and adsorbed sulfate extents in nuclei in different sulfate concentration
559 systems. Standard errors of measured SO_4^{2-}/Ca^{2+} ratios obtained from three independent
560 measurements

Conditions		SO_4^{2-}/Ca^{2+} ratios
1 mM	Total sulfate	$(2.7 \pm 0.4) \times 10^{-3}$
	Adsorbed sulfate	0
	Incorporated sulfate	$(2.7 \pm 0.4) \times 10^{-3}$
5 mM	Total sulfate	$(5.5 \pm 0.5) \times 10^{-3}$
	Adsorbed sulfate	0
	Incorporated sulfate	$(5.5 \pm 0.5) \times 10^{-3}$
10 mM	Total sulfate	$(9.1 \pm 1.4) \times 10^{-3}$
	Adsorbed sulfate	$(0.3 \pm 0.3) \times 10^{-3}$
	Incorporated sulfate	$(8.8 \pm 1.4) \times 10^{-3}$

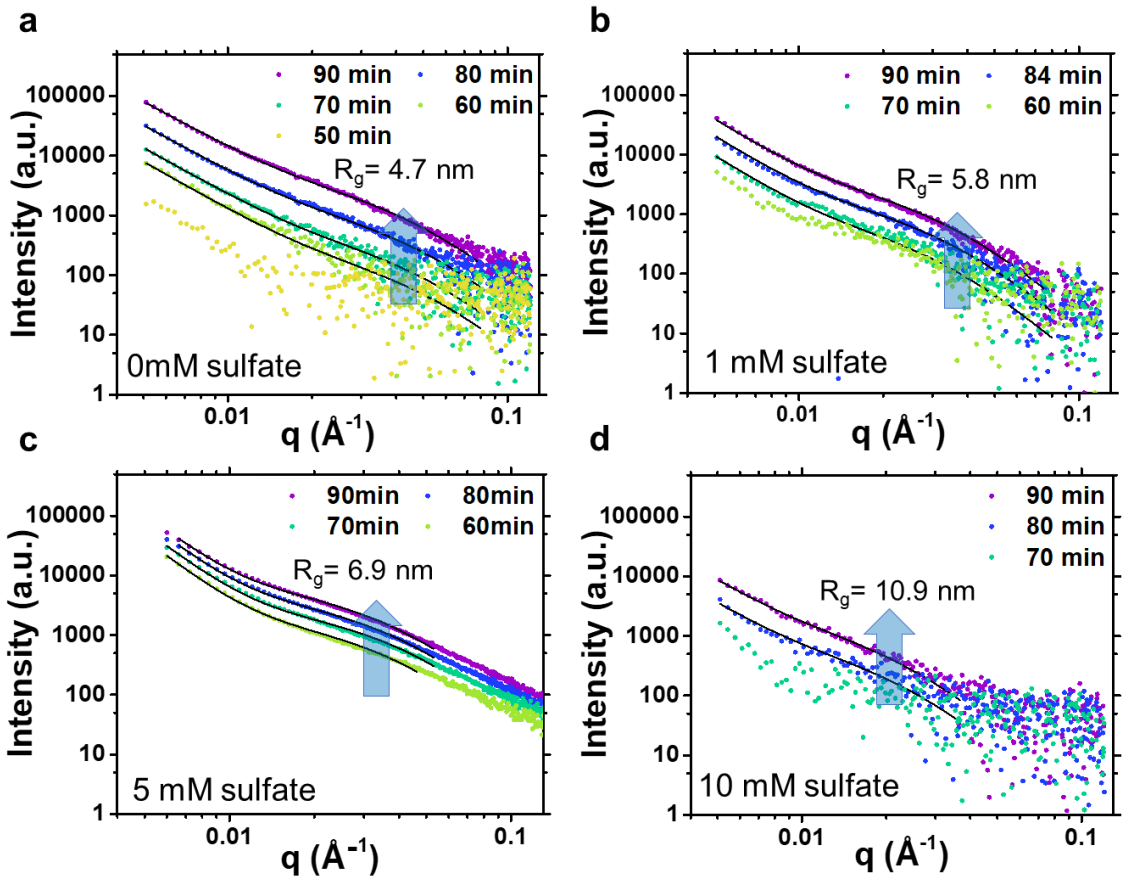

561

562 **Figure 1** Representative GISAXS patterns for four different sulfate concentrations: **a.** 0 mM,
563 **b.** 1 mM, **c.** 5 mM, and **d.** 10 mM. GISAXS patterns were obtained from line-cuts along 2D
564 scattering patterns' Yoneda wing, where the scattering intensities by particles on the surface were
565 most enhanced.[28] The induction time for 0, 1, 5, and 10 mM sulfate concentrations are 40, 50, 50,
566 and 60 mins. The blue arrows indicate the evolving trends of the bending locations in the GISAXS
567 pattern for each concentration (the bending location at a certain q is inversely proportional to the
568 particle size), which suggests that the particle growth effect is not significant. Duplicate GISAXS
569 experiments have been conducted. Replicate experiment result can be found in Figure S2.

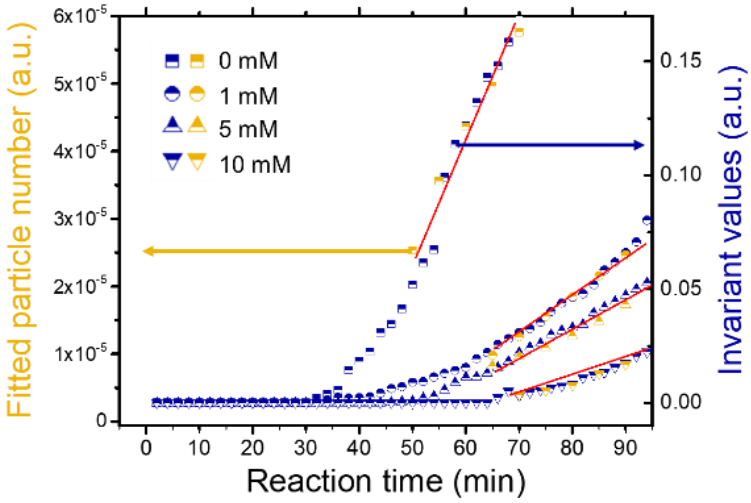

570

571 **Figure 2** Evolution of the fitted particle number (yellow, left y-axis) and invariant values
572 (blue, right y-axis) with reaction time for 0, 1, 5, and 10 mM sulfate conditions. The red lines are
573 linear regression analyses of the fitted particle number. The slopes of the linear regressions are the
574 nucleation rates. Duplicate GISAXS experiments have been conducted. Results from replicate
575 GISAXS experiment can be found in Figure S3.

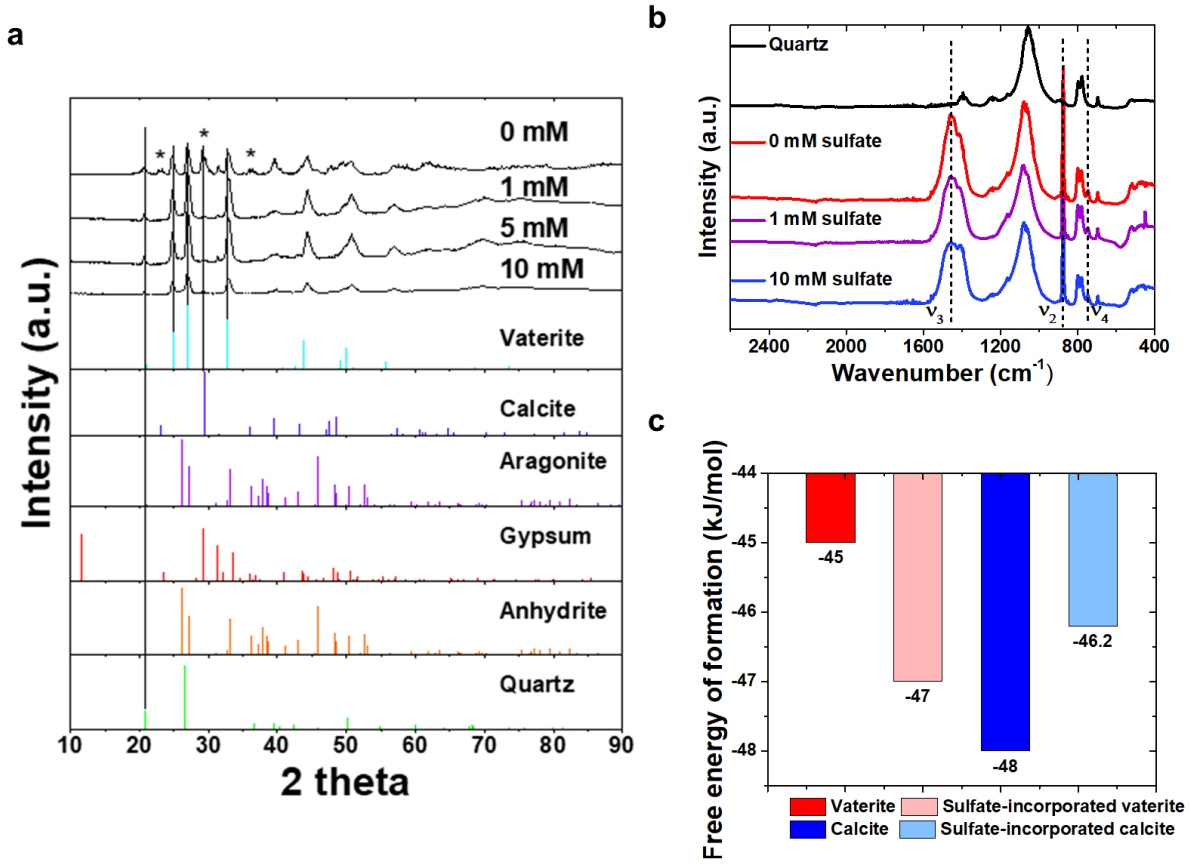

Figure 3 Phase identification of nuclei formed under different sulfate concentrations. **a**, GIWAXS results from nuclei formed on flat quartz substrate under different sulfate concentrations. The colored lines show peaks for different reference minerals. There is no gypsum or anhydrite formation. Vaterite is the $CaCO_3$ phase at 1 mM, 5 mM, and 10 mM sulfate concentrations. For 0 mM sulfate, the $CaCO_3$ is a mixed phase of calcite and vaterite. Asterisks (*) indicate the peaks from calcite. **b**, FTIR measurements of heterogeneous $CaCO_3$ nucleation on quartz powders. ν_2, CO_3 out of plane deformation mode; ν_3, asymmetric C–O stretching mode; and ν_4, OCO bending mode (in-plane deformation). **c**, Free energy of formation for vaterite, sulfate-incorporated-vaterite, calcite, and sulfate-incorporated-calcite.

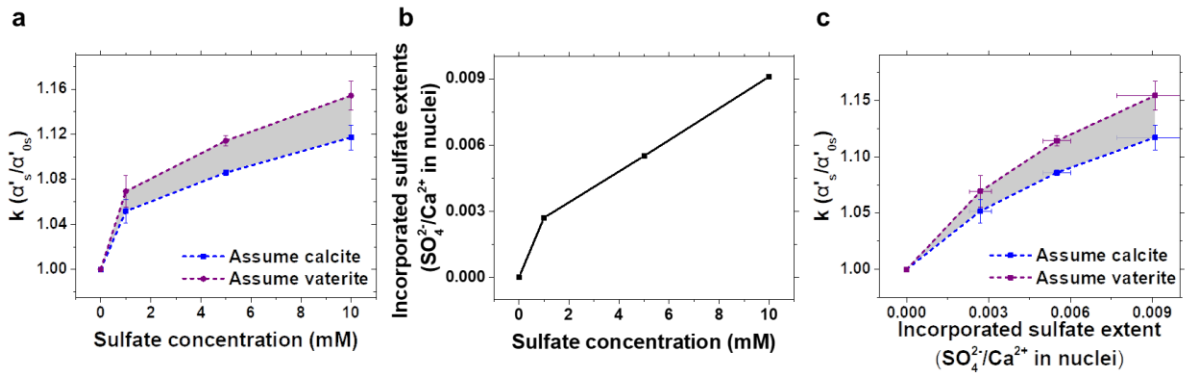

586

587 **Figure 4** Non-linear $CaCO_3$ effective interfacial energy evolution. If we assume the
588 polymorphs of $CaCO_3$ nuclei are calcite for our reaction system, we obtain the lower limit for the
589 *k* value calculation (blue curve). Assuming the polymorphs are vaterite gives the upper limit for *k*
590 values (purple curve). The grey area delineates the possible *k* values at different sulfate
591 concentrations/incorporated sulfate extents. **a**, Interfacial energy factors with respect to sulfate
592 concentrations. **b**, Evolution of incorporated sulfate extents with increasing aqueous sulfate
593 concentrations. **c**, Plot of interfacial energy factors with respect to incorporated sulfate extents.
594 Error bars in the symbols indicating *k* show the error when we used nucleation rates calculated
595 from duplicate GISAXS experiments. Error bars in the symbol indicating incorporated sulfate
596 extent (SO_4^{2-}/Ca^{2+} in nuclei) are the standard errors of measured incorporated sulfate extent (SO_4^{2-}
597 $/Ca^{2+}$ in nuclei) (obtained from three independent measurements).

598 **TOC**

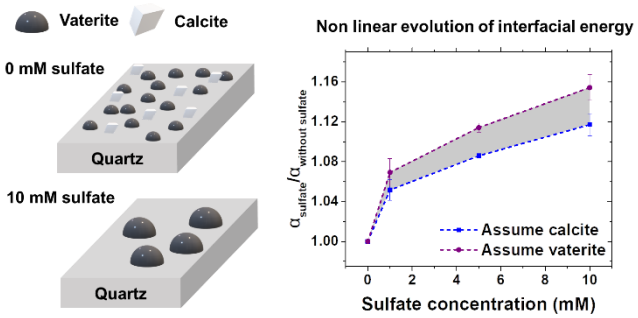

599

600